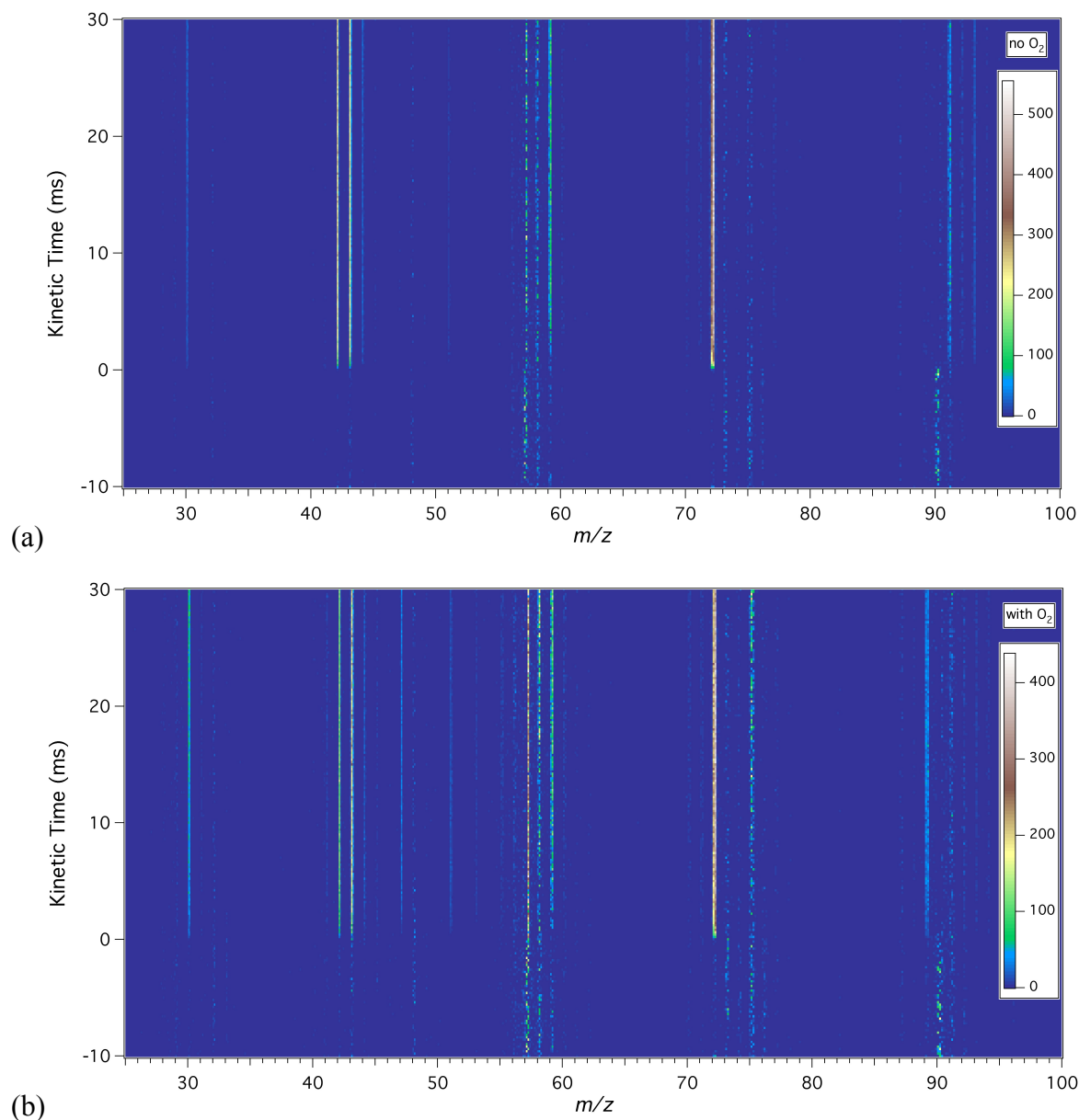


Supplementary Material for Zádor et al., Directly Measuring Reaction Kinetics of QOOH – a Crucial but Elusive Intermediate in Hydrocarbon Autoignition.



Supplementary Figure S1. Time-resolved photoionization mass spectrum in the (a) absence and (b) presence of oxygen obtained at 11.0 eV. The photolysis laser fires at 0 ms. The pre-photolysis background levels are subtracted. The plots are displayed such that product formation is emphasized, while the depletion of the reactants is masked (see color scale). Because of the high concentration of TBHP used in the experiments, the signals at $m/z=57$ and 58 arising from dissociative ionization of TBHP show artifacts caused by saturation of the TOF detector. This phenomenon is well-understood and does not affect other mass peaks. Therefore, signal at all other masses indicates time-dependent product formation.

Supplementary Material for Zádor et al., Directly Measuring Reaction Kinetics of QOOH – a Crucial but Elusive Intermediate in Hydrocarbon Autoignition.

Further assignments of observed signal in the MPIMS experiments

The photoionization of the parent TBHP ($m/z=90$), the minor masses and masses related to secondary chemistry seen in Supplementary Fig. S1 are discussed in this section. The identification of the chemical species was carried out by comparing the photoionization spectra of these masses to literature calibration spectra and adiabatic and/or vertical ionization energies. Some adiabatic and vertical ionization energies were also calculated in this work. The major masses that are related to QOOH chemistry are discussed in the main text.

The onset of photoionization at the parent mass of TBHP ($m/z=90$) is at ~ 9.1 eV, and the spectrum plateaus already at ~ 9.8 eV; the vertical IE literature value¹ is 10.24 eV. The calculated CBS-QB3 value for the AIE is 9.34 eV, and in the calculations the C–OOH bond of the cation is elongated to 1.80 Å (vs. 1.45 Å in the neutral), indicating likely photofragmentation into HO₂ and a *tert*-butyl cation. The lower ionization energy observed in the experiment compared to the calculation is likely caused by the thermal spread in the population, indicated by the shape of the photoionization spectrum (not presented here). Moreover, the uncertainty in the CBS-QB3 calculation can be on the order of ~ 0.1 eV.² The largest ion signal from photoionization of TBHP is at $m/z=57$ appearing around 9.5 eV, caused by HOO-loss during the photoionization process. The second largest peak is its ¹³C satellite at $m/z=58$, and the parent ion at $m/z=90$ is only the third largest peak; $m/z=75$ is another peak from TBHP, appearing upon methyl loss.

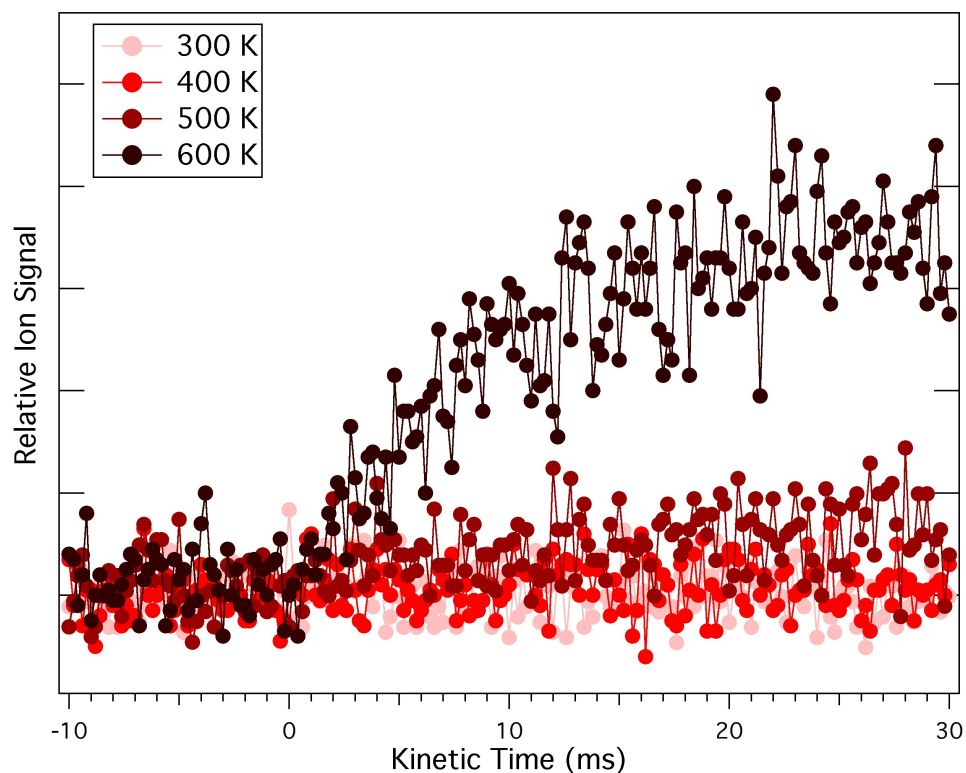
The time-resolved product signals at $m/z=91$ and 93 are most likely daughter ions from the chain-chlorination products ³⁵ClQOOH ($m/z=124$) and ³⁷ClQOOH ($m/z=126$), which, similarly to TBHP (“HQOOH”), are likely to lose HOO upon photoionization. The background-subtracted ratio of the integrated peaks is very close to $\sim 3:1$, reflecting the natural abundance of the ³⁵Cl and ³⁷Cl isotopes. The slight mass difference between ¹³CH₃(CH₃)₂COOH ($m/z=91.071$) and ³⁵ClQOOH ($m/z=91.031$) is also observable. Moreover, the intensity of these peaks gets smaller in the presence of O₂, because the O₂ + [•]QOOH reaction increasingly dominates the Cl₂ + [•]QOOH reaction (and also the [•]QOOH decomposition). There are several smaller product peaks with characteristic rise times of ~ 2.5 ms, slower than the rise time of DMO (~ 1 ms), signifying secondary chemistry. For instance, $m/z=59$ can be identified as a dissociative ionization product of *tert*-butanol ($m/z=74$) based on its calibration spectrum.³ *Tert*-butanol might be formed in secondary reactions of the *tert*-butoxy radical (RO), which itself can arise, e.g., in the ROO + ROO reaction. Smaller signals are observed at $m/z=51$ and 53, which can be

Supplementary Material for Zádor et al., Directly Measuring Reaction Kinetics of QOOH – a Crucial but Elusive Intermediate in Hydrocarbon Autoignition.

identified at ^{35}ClO and ^{37}ClO based on the ionization energy and the isotopic ratios, and are most likely the products of the $\text{ROO}^\bullet + \text{Cl}$ reaction. This reaction might be a further source of *tert*-butoxy.

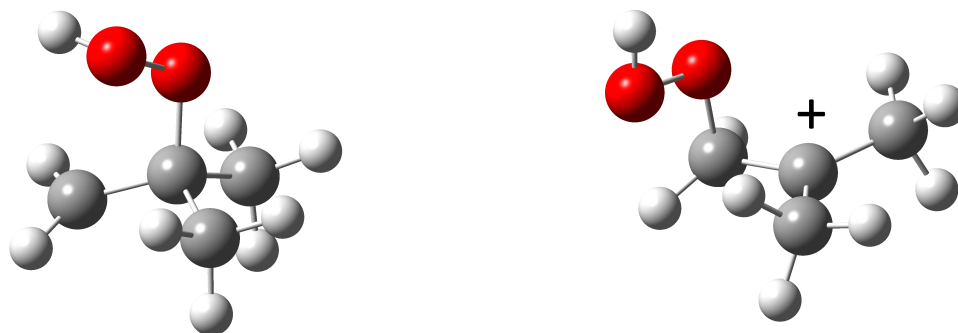
In the absence of O_2 , we observe a weak transient signal at $m/z = 15$, identified as methyl based on comparison of the $m/z = 15$ photoionization product spectrum with a literature methyl spectrum.⁴ A likely source of methyl is β -CC bond fission of *tert*-butoxy.⁵ This assignment is corroborated by the presence of acetone, the stable coproduct of the fission reaction, in the $m/z = 58$ product spectrum. A smaller peak that appears only in the presence of oxygen is $m/z=47$, that corresponds to the methylperoxy radical ($\text{CH}_3\text{OO}^\bullet$) based on the literature spectrum.⁶ A likely source is the $\text{CH}_3 + \text{O}_2$ reaction. However, the rise time is longer than those of 2,2-dimethyl oxirane and the $m/z=89$ fragment of $^\bullet\text{OOQOOH}$, supporting formation via secondary chemistry.⁵

Supplementary Material for Zádor et al., Directly Measuring Reaction Kinetics of QOOH – a
Crucial but Elusive Intermediate in Hydrocarbon Autoignition.



Supplementary Figure S2. Temperature dependent $m/z=56$ (isobutene) time profiles in the absence of oxygen in the TBHP + Cl system. Isobutene can be formed either via $^{\bullet}\text{QOOH}$ dissociation or in the direct HO_2 elimination step from ROO^{\bullet} , as shown in Fig. 1. We can exclude the former channel under our experimental conditions, because the rise of isobutene is slower than the rise of DMO (from decomposition of $^{\bullet}\text{QOOH}$) even at room temperature. Moreover, at 600 K chain chlorination of $^{\bullet}\text{QOOH}$, which would continuously form ROO^{\bullet} and $^{\bullet}\text{QOOH}$, can no longer compete with the decomposition of $^{\bullet}\text{QOOH}$. Therefore, the rise time of $m/z = 56$ reflects the ROO^{\bullet} decomposition rate. These observations demonstrate that ROO^{\bullet} dissociation at room temperature is too slow to affect the measurements of $^{\bullet}\text{QOOH}$ kinetics, or any of the experimental results.

Supplementary Material for Zádor et al., Directly Measuring Reaction Kinetics of QOOH – a
Crucial but Elusive Intermediate in Hydrocarbon Autoignition.

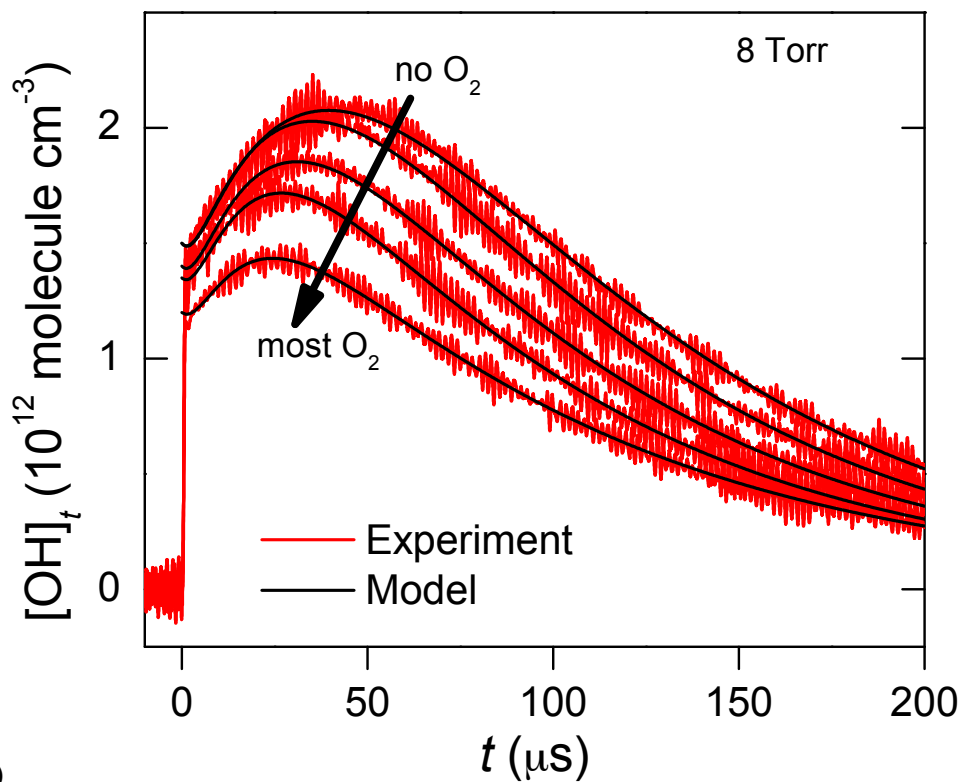


(a)

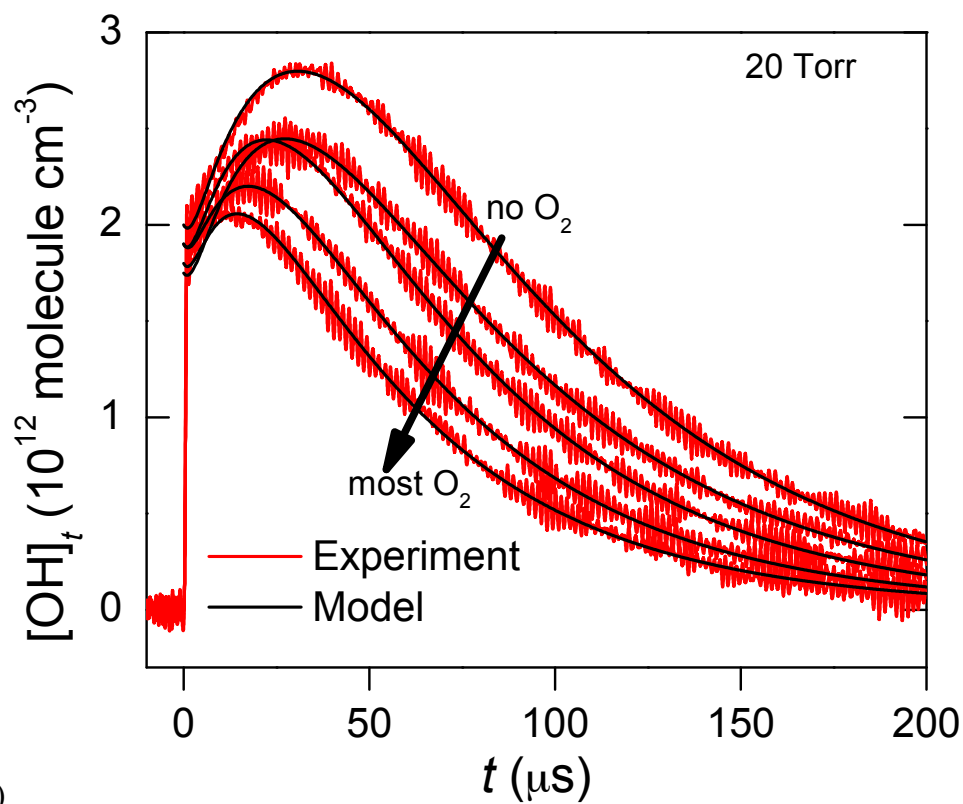
(b)

Supplementary Figure S3. The optimized geometry of (a) the 2-hydroperoxy-2-methylprop-1-yl radical ($\cdot\text{QOOH}$) and (b) its cation (Q^+OOH). In the cation the $-\text{OOH}$ group migrates to the $-\text{CH}_2$ carbon atom, thus forming a more stable, tertiary carbocation, creating poor Franck-Condon overlap with neutral $\cdot\text{QOOH}$.

Supplementary Material for Zádor et al., Directly Measuring Reaction Kinetics of QOOH – a
Crucial but Elusive Intermediate in Hydrocarbon Autoignition.

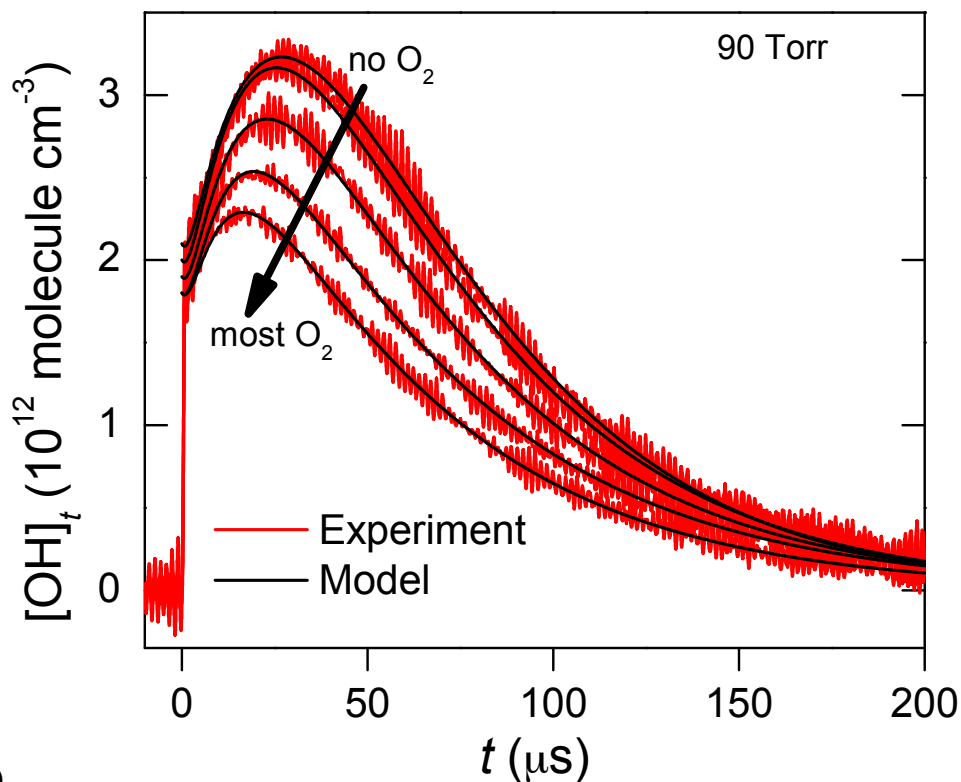


(a)



(b)

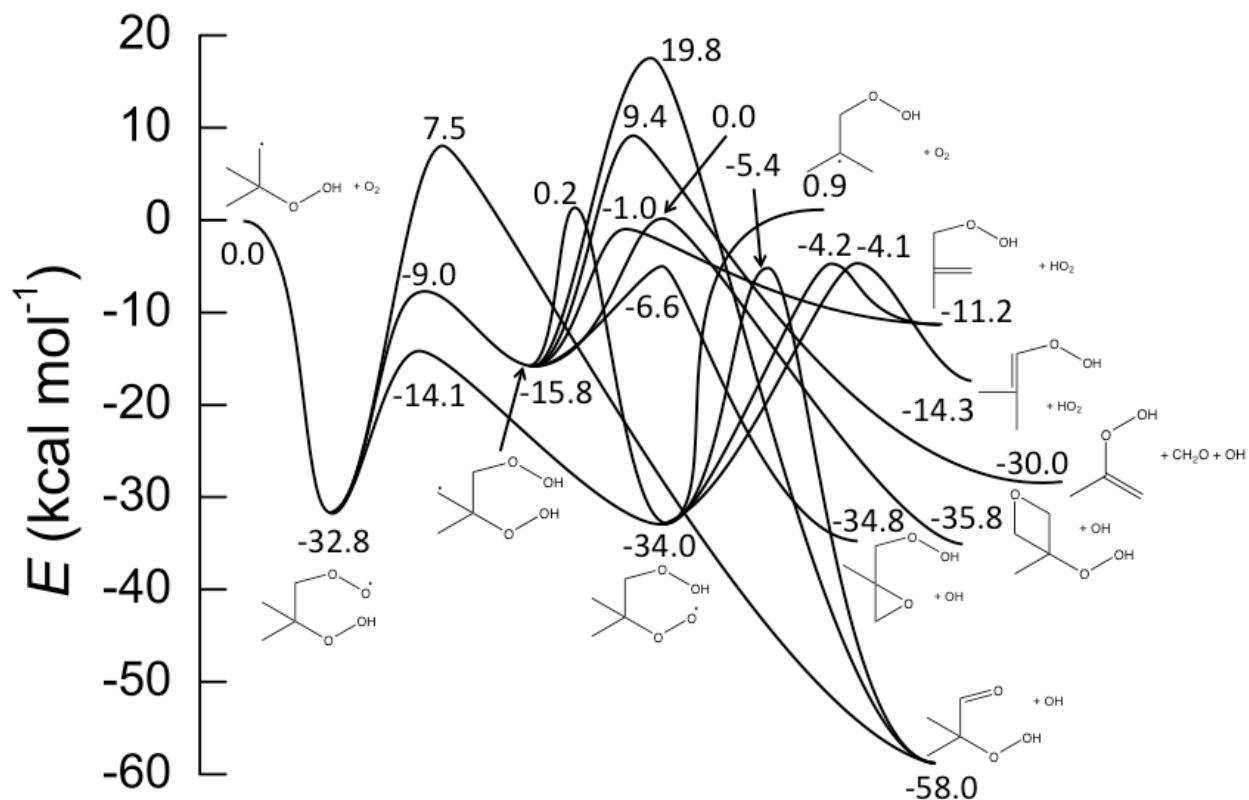
Supplementary Material for Zádor et al., Directly Measuring Reaction Kinetics of QOOH – a Crucial but Elusive Intermediate in Hydrocarbon Autoignition.



(c)

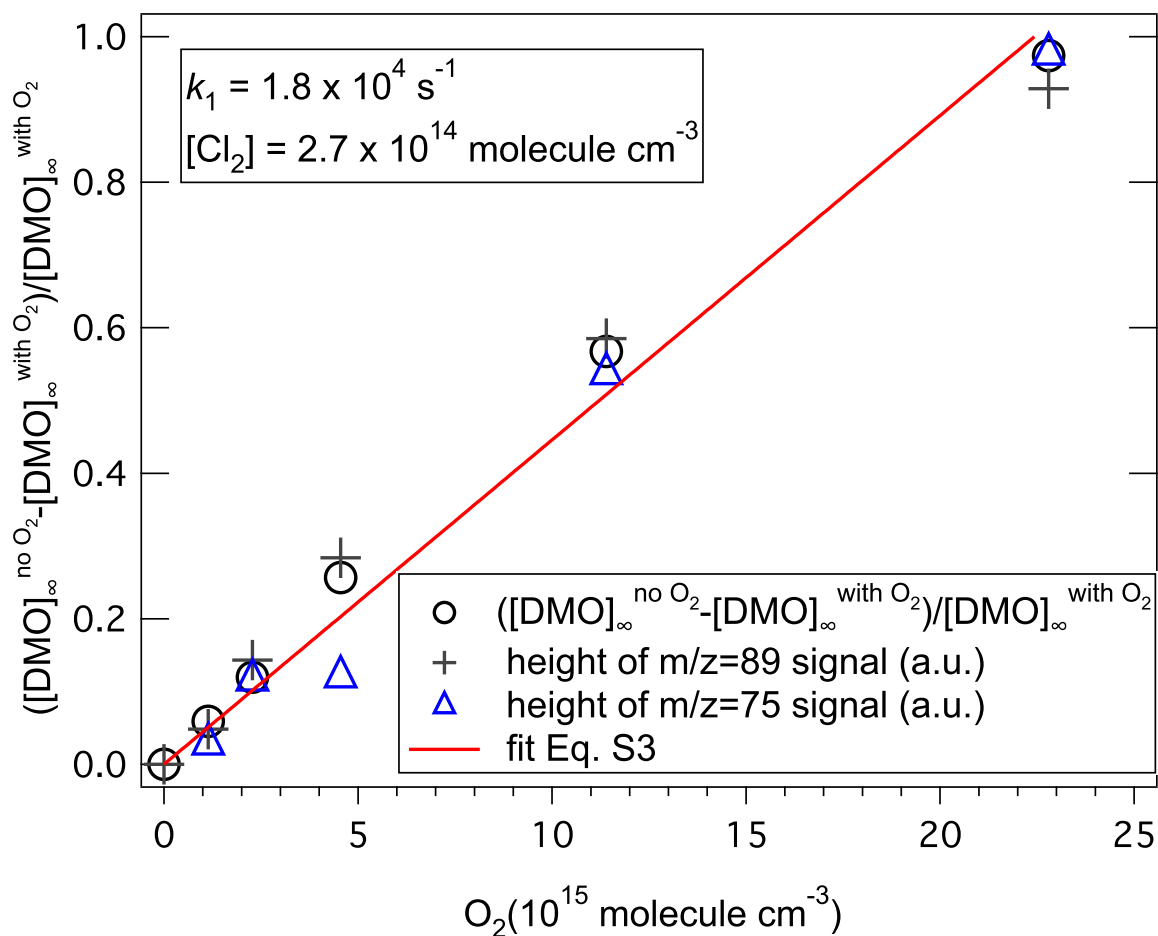
Supplementary Figure S4. The measured OH concentration-time profiles in the direct absorption experiments as a function of O₂ concentration at room temperature and at (a) 8, (b) 20 and (c) 90 Torr of total pressure using He as diluent, shown as the red lines. The solid black lines are the fits according to the mechanism described in the Supplementary Methods section. The experimental conditions can be found in Supplementary Table S2.

Supplementary Material for Zádor et al., Directly Measuring Reaction Kinetics of QOOH – a
Crucial but Elusive Intermediate in Hydrocarbon Autoignition.



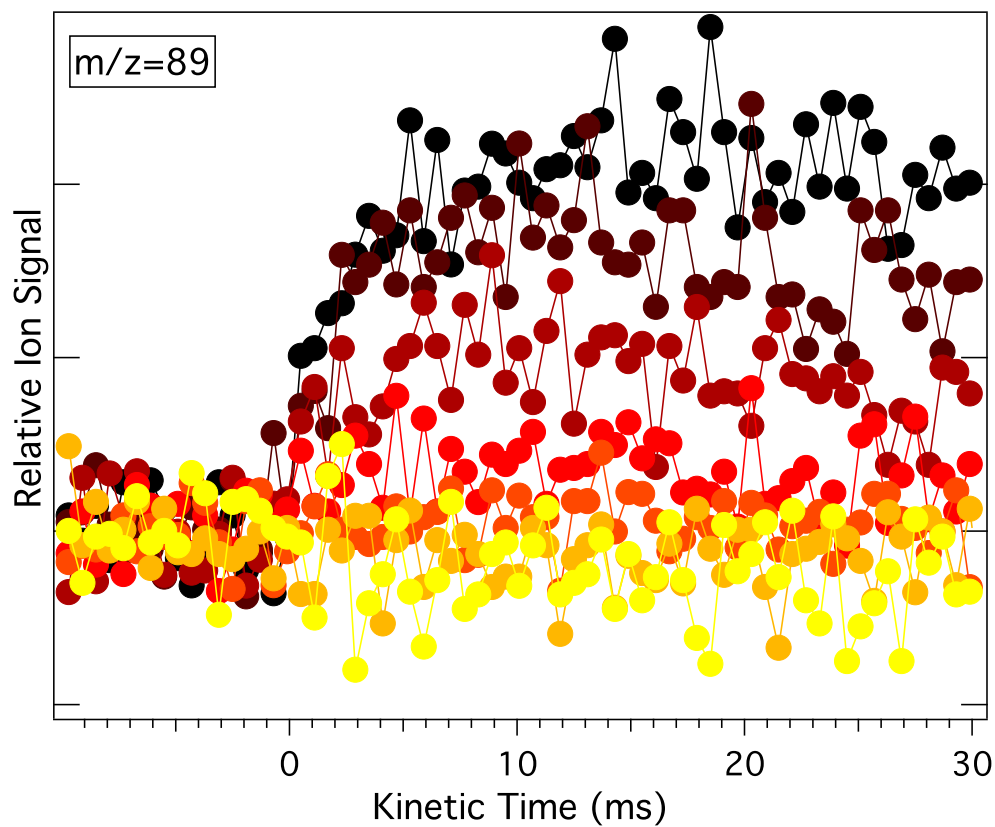
Supplementary Figure S5. The ZPE-corrected PES for the $\cdot\text{QOOH} + \text{O}_2$ reaction, calculated at the CBS-QB3 level of theory.

Supplementary Material for Zádor et al., Directly Measuring Reaction Kinetics of QOOH – a Crucial but Elusive Intermediate in Hydrocarbon Autoignition.

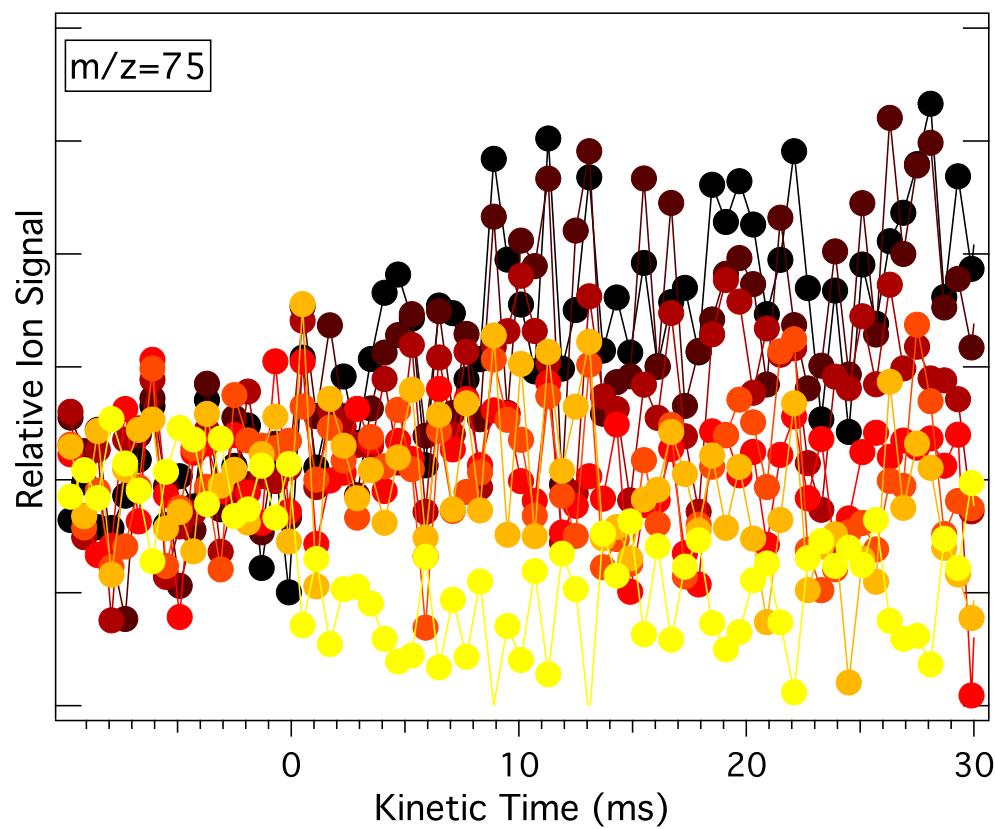


Supplementary Figure S6. The normalized change in the asymptotic DMO signal height ($m/z=72$) recorded at 11.0 eV at various O_2 concentrations, and the asymptotic signal heights for $m/z=75$ and 89 in arbitrary units. The linear fit is based on the expression in the Supplementary Methods section (Eq. S3).

Supplementary Material for Zádor et al., Directly Measuring Reaction Kinetics of QOOH – a
Crucial but Elusive Intermediate in Hydrocarbon Autoignition.

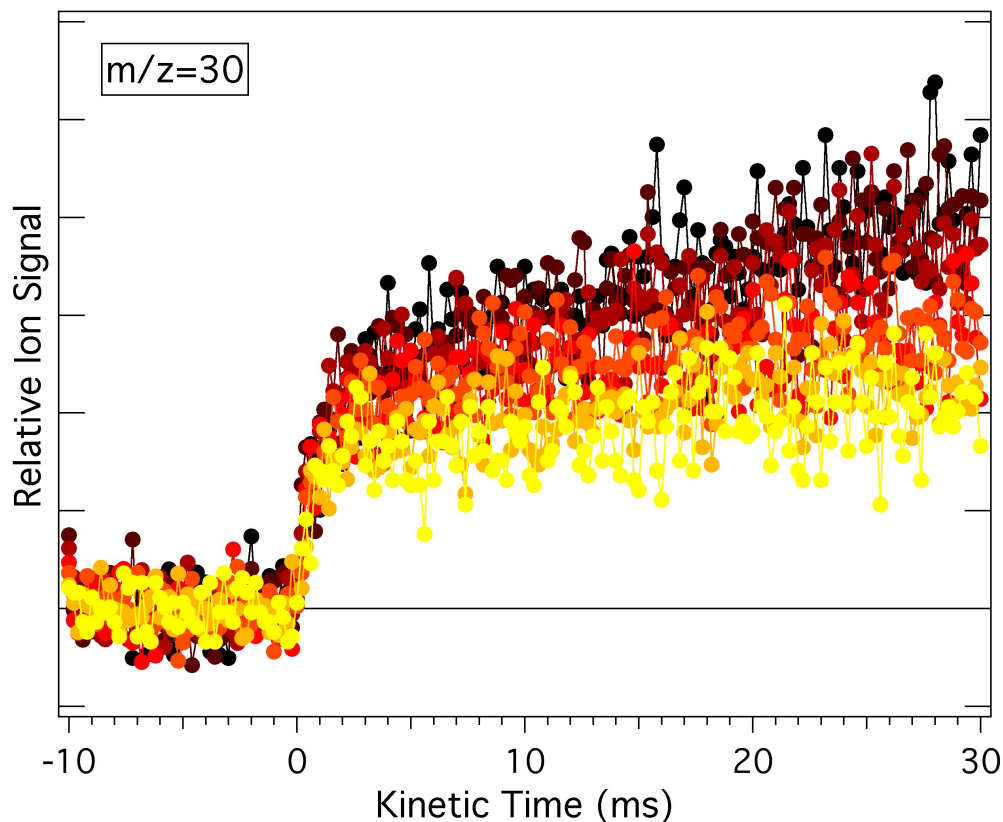


(a)



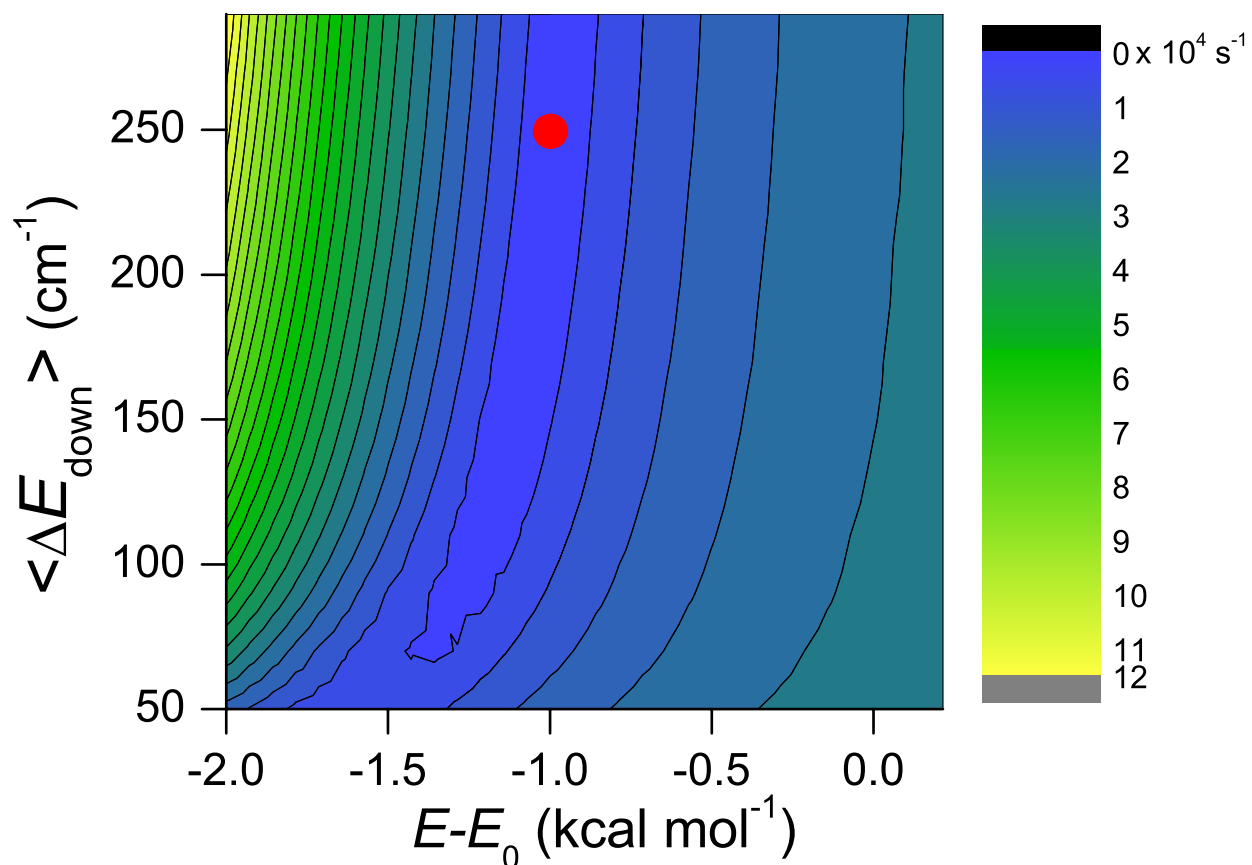
(b)

Supplementary Material for Zádor et al., Directly Measuring Reaction Kinetics of QOOH – a Crucial but Elusive Intermediate in Hydrocarbon Autoignition.



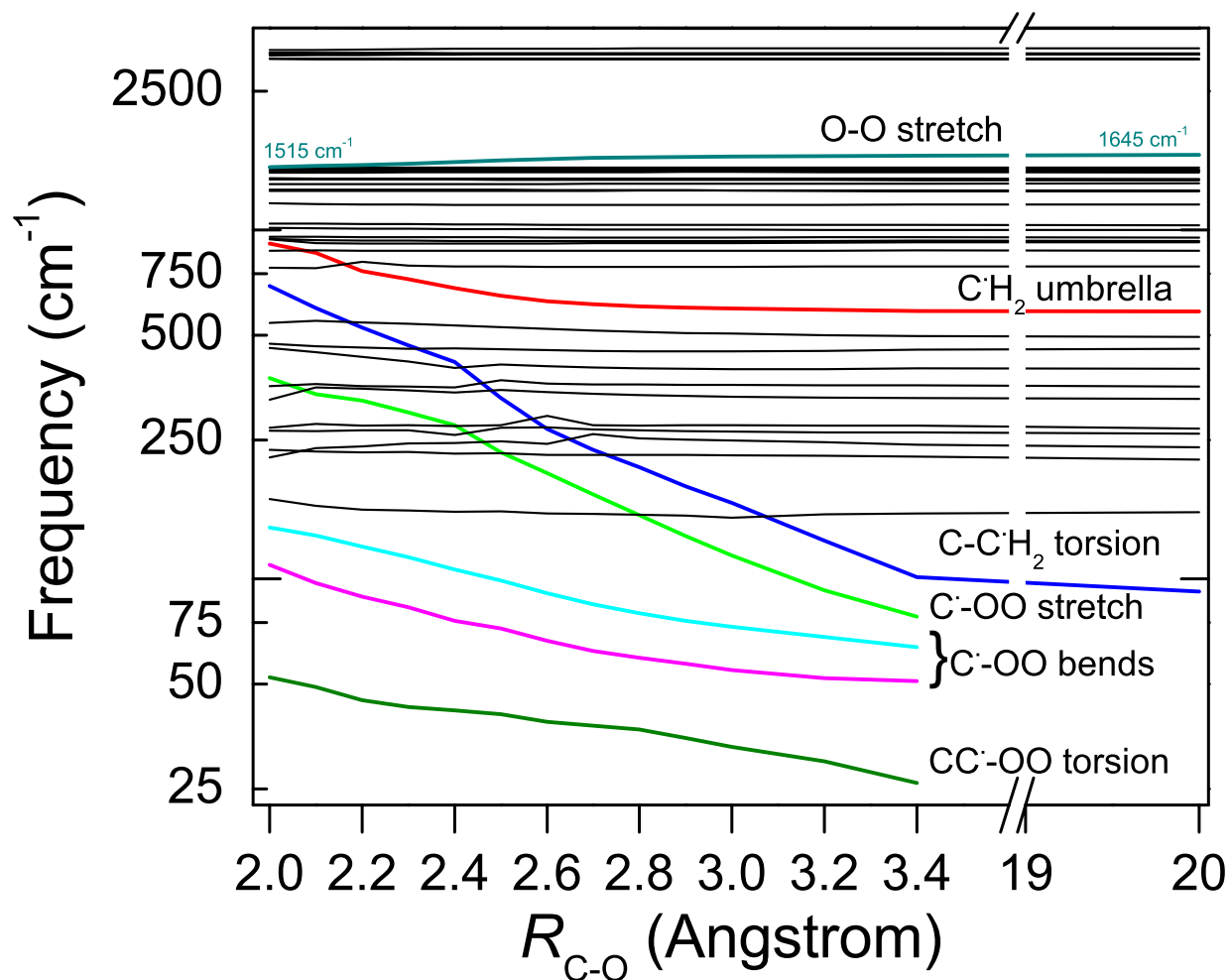
Supplementary Figure S7. The time traces of (a) $m/z=89$, (b) $m/z=75$ and (c) $m/z=30$ with increasing oxygen concentrations (in units of 10^{15} molecule cm^{-3}): 0, 1.14, 2.28, 4.55, 11.4, 22.8, 45.5 (corresponding to the color scale from yellow to black) recorded at 11.0 eV photon energy. The presented curves directly reflect the relative change in the concentration of the species that these ions originate from due to the variations in O_2 concentration. In the absence of O_2 the yellow curves were recorded, and the higher O_2 concentrations correspond to higher signals, shown in darker colors. Note that for $m/z=75$ the depletion (shown with the lightest color) in the absence of oxygen arising from dissociative ionization of TBHP was used to correct the signals in the other experiments. Here, the corrected curves are shown. The smaller S/N ratio is also a result of the required background subtraction. Signal at $m/z=30$ was identified as formaldehyde. Its yield is $\sim 10\%$ relative to DMO, and increases with increasing $[\text{O}_2]$. However, we were unable to explain these observations. Formaldehyde is most likely due to secondary chemistry.

Supplementary Material for Zádor et al., Directly Measuring Reaction Kinetics of QOOH – a Crucial but Elusive Intermediate in Hydrocarbon Autoignition.



Supplementary Figure S8. Absolute values of the average deviation between calculated and experimentally determined unimolecular dissociation rate coefficients k_1 of 2-hydroperoxy-2-methylprop-1-yl at the four pressures studied (8, 20, 60 and 90 Torr). The average deviation is shown as a function of the energy transfer parameter $\langle \Delta E_{\text{down}} \rangle$ and the variation of the barrier height for DMO + OH formation from the value obtained at the QCISD(T)/cc-PV ∞ Z//M06-2X/6-311++G(d,p) level. The red dot shows the best fit parameters: the barrier is 1.0 kcal mol⁻¹ lower than the calculated value, and the energy transfer parameter $\langle \Delta E_{\text{down}} \rangle$ is 250 cm⁻¹.

Supplementary Material for Zádor et al., Directly Measuring Reaction Kinetics of QOOH – a Crucial but Elusive Intermediate in Hydrocarbon Autoignition.



Supplementary Figure S9. The calculated CASPT2(5,7)/cc-pVDZ frequencies along the reaction coordinate in the QOOH + O_2 addition, with the most important and changing modes labeled. The lowest four frequencies at 3.4 Å are the ones corresponding to transitional modes.

Supplementary Material for Zádor et al., Directly Measuring Reaction Kinetics of QOOH – a Crucial but Elusive Intermediate in Hydrocarbon Autoignition.

Supplementary Methods

Fitting the OH profiles in the absorption experiments

The following chemical mechanism was used to analyze the experimental data in the absorption experiments. The rate coefficients are denoted as k_n , where n is the reaction number. The branching to COCl from photolysis of oxalyl chloride ((COCl)₂) is α , while β is the branching of the TBHP + Cl reaction to form QOOH.

reaction	$k(298\text{ K})$	Ref.
(COCl) ₂ + hv(266 nm) → α COCl + (2- α) CO + (2- α) Cl	$\alpha = 0.22 \pm 0.23$ @ 248 nm instantaneous	7
COCl + He → CO + Cl + He	$k_0 = (13.9 \pm 2.1) \times 10^{-15} \text{ cm}^3 \text{ molecule}^{-1} \text{ s}^{-1}$	7
QOOH → DMO + OH	k_1 , unknown	-
QOOH + O ₂ → OOQOOH	k_2 , unknown	-
TBHP + hv(266 nm) → <i>tert</i> -butoxy + OH	instantaneous	8
TBHP + Cl → QOOH + HCl	$\beta \times k_3$, β is unknown $k_3 \sim 7.7 \times 10^{-11} \text{ cm}^3 \text{ molecule}^{-1} \text{ s}^{-1}$	9
TBHP + Cl → ROO + HCl	$(1-\beta) \times k_3$	9
TBHP + OH → ROO + H ₂ O	$k_4 = (3.58 \pm 0.54) \times 10^{-12} \text{ cm}^3 \text{ molecule}^{-1} \text{ s}^{-1}$	8

The ODE system can be written as follows, considering [TBHP] and [O₂] constant, since these reactants are present in large excess.

$$d[\text{OH}]_t / dt = k_1[\text{QOOH}]_t - k_4[\text{TBHP}][\text{OH}]_t, \quad [\text{OH}]_0 = \text{oh}_0$$

$$d[\text{QOOH}]_t / dt = k_3\beta[\text{TBHP}][\text{Cl}]_t - k_1[\text{QOOH}]_t - k_2[\text{O}_2][\text{QOOH}]_t, \quad [\text{QOOH}]_0 = 0$$

$$d[\text{Cl}]_t / dt = k_0[\text{COCl}]_t - k_3[\text{TBHP}][\text{Cl}]_t, \quad [\text{Cl}]_0 = \text{cl}_0$$

$$d[\text{COCl}]_t / dt = -k_0[\text{COCl}]_t, \quad [\text{COCl}]_0 = \text{cocl}_0$$

Supplementary Material for Zádor et al., Directly Measuring Reaction Kinetics of QOOH – a Crucial but Elusive Intermediate in Hydrocarbon Autoignition.

The unknown parameters in the absence of O₂ are β and k_1 ; moreover, the uncertain concentration of TBHP is fitted as well. The latter is an uncertain parameter due to the difficulties arising in assessing its exact concentration in the gas phase when its aqueous solution is used in the bubbler. Therefore, the number of fitted parameters is three. Once k_1 is determined at a given pressure, k_2 can be determined by fitting the experimental [OH]-time profiles in the presence of O₂. β and the concentration of TBHP are fitted as well, in order to account for the slight variations in the flow rates. The lifetime of the Cl atoms is ~ 2 μ s or shorter under our experimental conditions.

The initial OH concentration was set to the experimental value of the sharp rise. Beyond that, the fits are insensitive to the absolute concentration of the OH radical, and also to k_4 . The latter is because fitting the TBHP concentration can fully compensate for it, moreover, the removal reaction of OH with TBHP only produces ROO + H₂O under our conditions.⁸ The details of the (COCl)₂ photodissociation only influence the curves at very early times, and do not have any significant effect on the results. The parameter that has a significant correlation with the fitted values for k_1 and k_2 is k_3 , for which we chose the value of 7.7×10^{-11} cm³ molecule⁻¹ s⁻¹ based on Ref.⁹. The error bounds for k_1 and k_2 shown in Figure 4a of the main manuscript include the range returned by varying the k_3 value by $\pm 30\%$.

The fitting was carried out with Mathematica.¹⁰ The analytical solution of the ODE was fitted repeatedly with various, substantially different, but physically meaningful initial parameter guesses. We found that the solution converged always to a unique solution.

Supplementary Material for Zádor et al., Directly Measuring Reaction Kinetics of QOOH – a Crucial but Elusive Intermediate in Hydrocarbon Autoignition.

Relative-rate determination of k_2 from the MPIMS experiments

For the numbering of the reactions, see the “Fitting the OH profiles in the absorption experiments” section above. In the MPIMS experiments QOOH loss happens due to

- unimolecular decomposition, k_1 : $\text{QOOH} \rightarrow \text{DMO} + \text{OH}$
- its reaction with O_2 , k_2 : $\text{QOOH} + \text{O}_2 \rightarrow \text{OOQOOH}$
- chain chlorination, k_5 : $\text{QOOH} + \text{Cl}_2 \rightarrow \text{ClQOOH} + \text{Cl}$

The chlorine atoms are regenerated in the chain chlorination step, and can in turn react with the excess TBHP partly to regenerate QOOH. Therefore, the apparent loss rate coefficient of QOOH in the chain chlorination step is only $k_5 \times (1 - \beta)$.

The asymptotic DMO concentration, which practically corresponds to the DMO concentration at the plateau in the time profile (see Fig. 2 in the main text), is, therefore:

$$[\text{DMO}]_{\infty} \propto \frac{k_1}{k_1 + k_2[\text{O}_2] + (1 - \beta)k_5[\text{Cl}_2]} \quad (\text{Eq. S1})$$

The ratio of two asymptotes, one at zero, and the other at nonzero O_2 concentration is, therefore:

$$\frac{[\text{DMO}]_{\infty}^{\text{with O}_2}}{[\text{DMO}]_{\infty}^{\text{no O}_2}} = \frac{K}{K + k_2[\text{O}_2]} \quad K = k_1 + (1 - \beta)k_5[\text{Cl}_2] \quad (\text{Eq. S2})$$

Rearranging the above expression yields:

$$\frac{[\text{DMO}]_{\infty}^{\text{no O}_2} - [\text{DMO}]_{\infty}^{\text{with O}_2}}{[\text{DMO}]_{\infty}^{\text{with O}_2}} = \frac{k_2}{K}[\text{O}_2] \quad (\text{Eq. S3})$$

which means that the plot of left-hand-side as a function of $[\text{O}_2]$ should yield a linear function, and its slope times K is equal to k_2 .

In the calculations we used $\beta = 0.18$ based on Supplementary Table S2 and $k_5 = 2.25 \times 10^{-11} \text{ cm}^3 \text{ molecules}^{-1} \text{ s}^{-1}$.¹¹ We have not considered the effect of wall loss in the above equations, which would appear as an additive term in the numerator of the last equation, and would result in a larger k_2 value. Therefore, our estimate for k_2 is a lower limit in this case.

Supplementary Material for Zádor et al., Directly Measuring Reaction Kinetics of QOOH – a Crucial but Elusive Intermediate in Hydrocarbon Autoignition.

Supplementary Table S1. The initial concentrations for the MPIMS experiments. All experiments were done at 298 K and 4 Torr.

$[\text{O}_2]$ (10^{15} cm^{-3})	$[\text{TBHP}]$ (10^{14} cm^{-3})	$[\text{Cl}_2]$ (10^{14} cm^{-3})	$[\text{Cl}]_0$ (10^{13} cm^{-3})
0.0	2.28	2.73	1.14
45.5	2.28	2.73	1.14
22.8	2.28	2.73	1.14
11.4	2.28	2.73	1.14
2.28	2.28	2.73	1.14
1.1	2.28	2.73	1.14
4.6	2.28	2.73	1.14

Supplementary Material for Zádor et al., Directly Measuring Reaction Kinetics of QOOH – a
 Crucial but Elusive Intermediate in Hydrocarbon Autoignition.

Supplementary Table S2. The fitted values and the initial concentrations for the absorption
 experiments. All experiments were done at (298±2) K.

P (Torr)	k_1 (10^4 s^{-1})	k_2 ($10^{-12} \text{ cm}^3 \text{ s}^{-1}$)	β	$[\text{O}_2]$ (10^{15} cm^{-3})	$[\text{TBHP}]$ (10^{15} cm^{-3})	$[\text{Cl}]_0$ (10^{13} cm^{-3})
90	3.7		0.18	0	6.52	2.85
		0.79	0.19	16	5.58	2.89
		0.69	0.17	36	5.23	2.89
		0.65	0.17	78	4.84	2.94
		0.40	0.15	145	5.15	2.90
		mean: 0.63				
60	3.6		0.19	0	7.11	3.09
		1.34	0.19	17	6.25	3.05
		0.90	0.20	37	6.67	3.05
		0.86	0.19	80	6.32	3.16
		0.67	0.18	149	6.52	3.17
		mean: 0.94				
20	2.8		0.18	0	5.41	2.60
		0.98	0.17	20	5.24	2.66
		0.69	0.16	44	5.48	2.52
		0.65	0.16	82	5.62	2.57
		1.31	0.17	9	4.87	2.61
		mean: 0.91				
8	2.2		0.15	0	4.00	2.12
		0.95	0.17	7	3.74	1.99
		1.11	0.16	16	3.46	2.01
		0.94	0.17	32	3.34	1.95
		0.72	0.15	54	3.05	1.66
		mean: 0.93				

Supplementary Material for Zádor et al., Directly Measuring Reaction Kinetics of QOOH – a Crucial but Elusive Intermediate in Hydrocarbon Autoignition.

Geometries of important species in Cartesian coordinates calculated at the M06-2X/6-311++G(d,p) level of theory

QOOH

C	0.026335	0.006246	0.014442
C	0.019053	0.000655	1.508672
O	1.379137	0.001687	2.010077
O	2.023660	1.202652	1.610173
C	-0.513933	-1.323670	2.050354
C	-0.741490	1.189045	2.081213
H	-0.304656	0.868796	-0.548341
H	0.427634	-0.846908	-0.519628
H	-0.441606	-1.336755	3.139469
H	0.062573	-2.158872	1.648603
H	-1.558999	-1.444452	1.760569
H	-0.697188	1.167645	3.171477
H	-1.786966	1.146775	1.767227
H	-0.305465	2.124992	1.730959
H	2.560263	0.902455	0.866168

TS(QOOH = DMO + OH)

C	0.022136	0.003687	0.009263
C	-0.014572	0.00947	1.488336
O	1.379421	0.024337	1.322327
O	2.085518	0.044431	2.880399
C	-0.505391	-1.264219	2.148078
C	-0.546435	1.276069	2.130187
H	0.075674	0.936158	-0.534787
H	0.112604	-0.930267	-0.52716
H	-0.189459	-1.269241	3.192497
H	-0.074116	-2.135515	1.653061
H	-1.594992	-1.324325	2.103313
H	-0.237656	1.302626	3.175976
H	-1.636911	1.302652	2.076145
H	-0.140468	2.154703	1.625883
H	2.88497	0.500631	2.588314

Supplementary Material for Zádor et al., Directly Measuring Reaction Kinetics of QOOH – a Crucial but Elusive Intermediate in Hydrocarbon Autoignition.

References used in the supplementary material

- [1] C. Batich and W. Adam, *Tetrahedron Lett.*, 1974, 1467-1470.
- [2] J. A. Montgomery, M. J. Frisch, J. W. Ochterski and G. A. Petersson, *J. Chem. Phys.*, 1999, **110**, 2822-2827.
- [3] M. F. Xie, Z. Y. Zhou, Z. D. Wang, D. N. Chen and F. Qi, *Int. J. Mass Spectrom.*, 2010, **293**, 28-33.
- [4] J. D. Savee, S. Soorkia, O. Welz, T. M. Selby, C. A. Taatjes and D. L. Osborn, *J. Chem. Phys.*, 2012, **136**.
- [5] C. Fittschen, H. Hippler and B. Viskolcz, *Phys. Chem. Chem. Phys.*, 2000, **2**, 1677-1683.
- [6] G. Meloni, P. Zou, S. J. Klippenstein, M. Ahmed, S. R. Leone, C. A. Taatjes and D. L. Osborn, *J. Am. Chem. Soc.*, 2006, **128**, 13559-13567.
- [7] B. Ghosh, D. K. Papanastasiou and J. B. Burkholder, *J. Chem. Phys.*, 2012, **137**, #164315.
- [8] M. Baasandorj, D. K. Papanastasiou, R. K. Talukdar, A. S. Hasson and J. B. Burkholder, *Phys. Chem. Chem. Phys.*, 2010, **12**, 12101-12111.
- [9] N. Choi, M. J. Pilling, P. W. Seakins and L. Wang, *Phys. Chem. Chem. Phys.*, 2006, **8**, 2172-2178.
- [10] I. Wolfram Research, Wolfram Research, Inc., Champaign, Illinois, 2010.
- [11] A. J. Eskola, V. A. Lozovsky and R. S. Timonen, *Int. J. Chem. Kinet.*, 2007, **39**, 614-619.